Astronomy & Astrophysics manuscript no. aa60918-26
November 4, 2026
©ESO 2026

The ALMA survey to Resolve exoKuiper belt Substructures (ARKS)

XII. Constraints on large bodies embedded in discs

M. R. Jankovic[1,⋆], A. V. Krivov[2], T. D. Pearce[3,4], A. A. Sefilian[5], M. C. Wyatt[6], E. Chiang[7], C. del Burgo[8,9], Y. Han[10], J. Jovicic[11], S. Marino[12], B. Zawadzki[13], A. M. Hughes[13], T. Löhne[2], P. Luppe[3], J. P. Marshall[14], Th. Henning[15], H. E. Schlichting[16], S. Mac Manamon[3], N. Pawellek[17,18], and D. J. Wilner[19]

(Affiliations can be found after the references)

Received MM DD, YEAR; accepted MM DD, YEAR

ABSTRACT

Context. The ALMA survey to Resolve exoKuiper belt Substructures (ARKS) presents detailed constraints on structure and properties of a sample of 24 debris discs at millimetre wavelengths, including measurements of vertical thicknesses for a subsample of discs.
Aims. We estimated sizes and total masses of large bodies that feed collisional cascades producing the observed millimetre dust in 11 ARKS discs with a well constrained vertical thickness. Separately, we estimated the sizes and total masses of large bodies that could be gravitationally stirring these discs, assuming that such stirring is the origin of the vertical thickness.
Methods. We used a semi-analytic particle-in-a-box collisional model and a semi-analytic model of stirring through gravitational scattering. We accounted for the dependence of collisional damping efficiency on the average collision velocity.
Results. We find that planetesimals feeding the collisional cascades are less than 20 km in size, while the total masses in the planetesimals are lower than 200 $M_\oplus$. There is a good agreement between minimum disc masses inferred from millimetre and infrared observations. The hypothetical stirrers are always larger in size than the planetesimals, but they do not necessarily contain most of the disc mass.
Conclusions. In agreement with previous work, the observed dust masses can be explained by steady-state collisional models with reasonable disc masses. The measured vertical scale-heights can be explained by gravitational stirring from embedded large bodies of reasonable properties. However, more advanced models are needed to address the observed non-Gaussian vertical profiles, along with the dependence of disc scale-height on particle size and stellocentric distance.

Key words. minor planets, asteroids: general – circumstellar matter – planetary systems

arXiv:2611.04976v1 [astro-ph.EP] 3 Nov 2026

1. Introduction

Cold dusty discs surround many main sequence stars. The dust is believed to be continually produced in large debris collisions that make up the bulk of the discs' masses, but that cannot be directly detected (Wyatt 2008; Krivov 2010; Matthews et al. 2014; Hughes et al. 2018; Wyatt 2020; Marino 2023; Pearce 2026). These large bodies are analogous to asteroids, Kuiper belt objects, and comets in the Solar System, and the small dust is key to our understanding of these bodies around other stars.

Using models of collisional cascades and measurements of dusty disc properties, it is possible to estimate the sizes and the total masses of the large bodies whose collisions produce the dust. We refer to these bodies as planetesimals. Current models predict that the size distribution of particles in a debris collisional cascade approximately follows a broken power law (e.g. O'Brien & Greenberg 2003; Pan & Sari 2005; Pan & Schlichting 2012; Thébault et al. 2003; Krivov et al. 2006). The observed dust mass can be extrapolated using the power-law size distribution to find the mass contained in the cascade as a function of the size of the largest bodies in the cascade. The size of the largest bodies in the cascade can be estimated as the size at which the collisional fragmentation timescale equals the system age. This timescale can be estimated through a simple particle-in-a-box model (Wyatt & Dent 2002). There might be bodies in the disc that are larger than those in the cascade, but they have longer fragmentation timescales and typically they have not yet collided. Smaller bodies, on the other hand, fragment and get removed from the system by radiation forces and/or a stellar wind on timescales shorter than the system age. In turn, they need to be replenished by larger bodies for the cascade to remain observable. With this approach, the so-called collisional mass of a debris disc can be estimated (e.g. Quillen et al. 2007; Krivov & Wyatt 2021; Pearce et al. 2025).

Furthermore, dusty discs may also contain (dwarf) planets that gravitationally stir and/or shape the discs. From resolved debris disc structures, dynamical constraints can be placed on the size and the number of these large bodies. Broadly speaking, there are two main system architectures that are typically explored. It can be assumed that large bodies within the disc viscously stir planetesimals and the dust (Ida & Makino 1993). Such bodies could either have formed in the protoplanetary disc phase (Krivov & Booth 2018), or their accretion may be ongoing throughout the debris disc evolution (Kenyon & Bromley 2002, 2004, 2008, 2010). In the former case, simple semi-analytic models can be used to relate disc observables to the sizes and the total mass of the stirrers (e.g. Quillen et al. 2007; Daley et al. 2019; Matrà et al. 2019; Terrill et al. 2023). On the other hand, the bodies stirring and shaping debris discs could be outside the discs, affecting discs via scattering as well as secular and resonant interactions. Such external perturbers could be closer to the star than the disc (e.g. Costa et al. 2024; Pearce et al. 2024; Sefilian 2024), farther away (e.g. Nesvold et al. 2017; Stuber et al. 2023), or both (Boley et al. 2012; Farhat et al. 2023).

⋆ E-mail: marija.jankovic@ipb.ac.rs

In this work, we focus on the former set-up, with hypothetical stirrers embedded in discs.

Recently, the Atacama Large Millimeter/submillimeter Array (ALMA) survey to Resolve exoKuiper belt Substructures (ARKS; Marino et al. 2026a) measured the structure of 24 debris discs in unprecedented detail at millimetre wavelengths. In the paper dedicated to the characterisation of the disc's vertical structures, Zawadzki et al. (2026) presented an analysis of a subsample of particularly well-resolved ARKS discs, inferring the sizes of bodies and disc masses required to stir the ARKS discs to their present-day vertical thicknesses. Based on assumptions of a balance between stirring and efficient collisional damping, they found the total mass of stirrers to range between 0.83 and 114 $M_\oplus$. However, for some of the discs, the corresponding stirring timescale was found a posteriori to be longer than the estimated system age. Additionally, for some of the discs, these dynamical masses are smaller than the minimum masses previously derived (albeit the latter have been estimated using different observational data, and also not for all of the ARKS discs; Krivov & Wyatt 2021).

In this paper, we expand upon both the collisional and the dynamical constraints on large bodies hiding in ARKS discs. We consider these constraints independently, assuming that the planetesimals feeding the collisional cascades and the stirrers may be two distinct populations of large bodies. In Sect. 2, we describe the dataset characterising our chosen sample of discs. In Sect. 3, we present the constraints placed on bodies in the collisional cascades. In Sect. 4, we revisit the constraints placed on the large bodies stirring the discs. In Sect. 5, we bring together the two sets of constraints and discuss our results. In Sect. 6, we present our conclusions.

2. Data

We considered a sample of 11 discs with well-constrained vertical structure, originally presented in Zawadzki et al. (2026). The data we used, which are summarised in Table A.1, comprise a subsample of 24 discs analysed in the (sub)millimetre in the ARKS programme (Marino et al. 2026a). We adopted stellar masses (M_*), stellar luminosities (L_*), stellar ages ($t_{\rm age}$), and fractional luminosities (f) from Table 1 of Marino et al. (2026a). In their work, Marino et al. (2026a) fit the discs' observations with a simple parametric Gaussian model of dust surface density and constant opacity. From Table B.1 in their work, we adopted the stellocentric radii of peak density (r, centre of the fitted Gaussian) and disc widths (Δr, FWHM of the fitted Gaussian), and the dust masses ($M_{\rm dust}$). The dust masses are derived by Marino et al. (2026a) assuming a power-law size distribution with a slope of $q = 3.5$, with grains from 1 μm up to 1 cm contributing to the observed flux. In this work, we assumed a slightly steeper size distribution at these dust sizes (see Sect. 3.3). We checked that changing the slope in the derivation of the dust mass to our theoretical one would only change the dust mass by 10-15 %; thus, we opted to neglect this small discrepancy.

For the disc aspect ratios (h), we adopted values from Table 3 of Zawadzki et al. (2026). We only considered the 11 discs whose aspect ratios had been well constrained with parametric modelling to keep our analysis uniform. The modelling defines the disc scale-height as the half width at half maximum of the vertical density profile, and this scale-height is assumed to be directly proportional to stellocentric distance within each disc (see Eq. 1 in Zawadzki et al. 2026). The aspect ratio, defined as the ratio of the scale-height and stellocentric distance, is therefore assumed to be constant and does not depend on the radius within the disc.

3. Constraints on planetesimals

In this section, we interpret the discs in our sample as steady-state collisional cascades. We assume that the observed disc aspect ratios determine collision velocities and that the velocities have been constant throughout the system lifetimes. Accounting for velocity evolution due to stirring by embedded large bodies would not significantly change our results (see Sect. 5.2.4). We calculated the collision velocities and the sizes of the projectiles that destroy targets of different sizes, and, ultimately, the collisional lifetimes of particles in the disc. By comparing the collisional lifetimes with system ages for each disc, we were able to place constraints on the sizes of the bodies feeding the cascades.

3.1. Collision velocity

Debris discs are made up of large numbers of bodies on randomised orbits. We assumed all the discs in our sample to be axisymmetric, such that the orbital angles are uniformly distributed (but see Lovell et al. 2026). Based on simulations of gravitational interactions among planetesimals and based on observations of the Kuiper belt (Ida & Makino 1992; Lissauer & Stewart 1993; Brown 2001), it is reasonable to expect that the distributions of the orbital eccentricity and inclination in the observed debris discs might be close to the Rayleigh distribution (see, however, Zawadzki et al. 2026; Chiang et al. 2026). If that is the case, in a disc with an average particle orbital eccentricity, e, and inclination, i, the average relative velocity with which particles with similar semi-major axes approach each other (Lissauer & Stewart 1993) is given by

$$v_{\rm rel} = \sqrt{\frac{5}{4}\langle e^2\rangle + \langle i^2\rangle}\, v_{\rm K}, \tag{1}$$

where $v_{\rm K}$ is the local Keplerian velocity. We further assumed that $\sqrt{\langle e^2\rangle} \approx 2\sqrt{\langle i^2\rangle}$. This is expected if the origin of the inclination dispersion is gravitational stirring by large bodies present in the disc (in the dispersion-dominated regime, Ida & Makino 1992). Then, $v_{\rm rel}$ is determined only by the average inclination.

For a Rayleigh distribution of inclinations, the vertical spatial distribution of particles is Gaussian, and the average inclination is related to the disc aspect ratio as $\sqrt{\langle i^2\rangle} = \sqrt{2}h$ (Matrà et al. 2019). Combining all of these equations, we can obtain a simple relationship between h and $v_{\rm rel}$,

$$v_{\rm rel} = 2\sqrt{3}h v_{\rm K}. \tag{2}$$

Zawadzki et al. (2026) found that for many of the ARKS discs the vertical structure at mm wavelengths is not, in fact, Gaussian. They reported the aspect ratio corresponding to half-width half-maximum of the vertical structure. We assumed that accounting for a different vertical distribution or the slightly different aspect ratio definition would only change $v_{\rm rel}$ by a factor of an order of unity and, thus, we neglected this factor in favour of Eq. (2), which is widely adopted (e.g. by Zawadzki et al. 2026).

With the aspect ratios, stellar masses, and the central disc radii obtained as described in Sect. 2, $v_{\rm rel}$ ranges between 40 m s^{-1} and 2600 m s^{-1} for the discs in our sample (see Table A.1). These collision velocities are higher than the escape velocities from the planetesimals feeding the cascades, whose sizes we present further below (the escape velocity is $\sim$ 10 m s^{-1} for

rocky 10 km-sized planetesimals). This means that the gravity of the planetesimals does not significantly influence the collision rates and the role of gravitational focusing can be neglected within the collisional cascade.

3.2. Projectile-to-target mass ratio

Collisional fragmentation occurs if the impact energy is higher than the critical energy to disrupt the target. Disruptive or catastrophic collisions are those where the largest surviving body after the collision has less than half of the mass of the target. At a fixed collision velocity, $v_{\rm rel}$, there is a minimum mass of a projectile, $m_{\rm c}$, that can collisionally disrupt the target of mass $m_{\rm t}$, and if $m_{\rm c} \ll m_{\rm t}$ (e.g. Krivov et al. 2006), we have

$$\frac{m_{\rm c}}{m_{\rm t}} = \frac{2Q^*_{\rm D}}{v^2_{\rm rel}}, \tag{3}$$

where $Q^*_{\rm D}$ is the specific critical disruption energy that depends on the target size, composition, and the collision velocity (e.g. Benz & Asphaug 1999). The critical projectile size (radius) is given by $s_{\rm c} = s_{\rm t}(2Q^*_{\rm D}/v^2_{\rm rel})^{1/3}$, for the target size, $s_{\rm t}$.

For the specific critical disruption energy, we adopted

$$Q^*_{\rm D}(s, v_{\rm rel}) = \left(Q_{\rm s}\left(\frac{s}{s_{\rm s}}\right)^{b_{\rm s}} + Q_{\rm g}\left(\frac{s}{s_{\rm g}}\right)^{b_{\rm g}}\right)\left(\frac{v_{\rm rel}}{v_0}\right)^{b_{\rm v}}, \tag{4}$$

where s is the particle size (radius), $Q_{\rm s} = Q_{\rm g} = 5 \times 10^6$ erg g^{-1} are the reference values in the strength and the gravity regime, respectively, at the reference sizes, $s_{\rm s} = 1$ m and $s_{\rm g} = 1$ km, $b_{\rm s} = -0.37$ and $b_{\rm g} = 1.38$ are the slopes of the size-dependence in the strength and the gravity regime, $v_0 = 3$ km s^{-1} is the reference velocity, and $b_{\rm v} = 0.5$ is the slope of the velocity-dependence (all values for basalt; Benz & Asphaug 1999; Stewart & Leinhardt 2009). For very large bodies ($\gtrsim 100$ km) the specific energy required to overcome self-gravity exceeds the above $Q^*_{\rm D}$. An additional term can be included to account for this (Leinhardt & Stewart 2009; Löhne et al. 2017). In this work we find planetesimals are small enough to neglect this term.

Figure 1 shows the resulting critical projectile-to-target mass ratio as a function of target size for our sample of debris discs. We find that that the critical mass ratios for mm-sized grains are in the range of $10^{-3} - 1$, meaning they indeed fragment in collisions with smaller or at least with similar-size particles. In some discs, for smallest and largest sizes the ratio $2Q^*_{\rm D}/v^2_{\rm rel}$ is larger than unity. We cut off the curves in Fig. 1 for such parameters because Eq. (3) is no longer valid and the ratio no longer represents the projectile-target mass ratio.

Finally, note that these results depend on the assumed material composition and porosity. For example, if the dust and the planetesimals are icy, they are disrupted more easily (Benz & Asphaug 1999) and their critical projectile sizes would be even smaller.

3.3. Size distribution in steady-state

To model the size distribution in a collisional cascade at the steady-state, we followed the model of Wyatt et al. (2011), which is similar to the model from Löhne et al. (2008). The model predicts a size distribution that is a broken power law. A collisional cascade that is at steady-state and in which particle strength depends on particle size as a power law ($Q^*_{\rm D} \propto s^b$) has a size

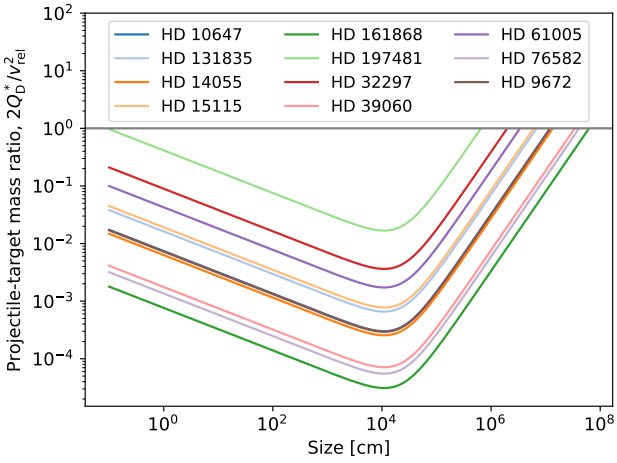


Fig. 1. Critical projectile-to-target mass ratio as function of target size for the discs in our sample, obtained using Eqs. (2), (3), and (4), and using data provided in Table A.1. The horizontal gray line indicates where $2Q^*_{\rm D}/v^2_{\rm rel} = 1$.

distribution that is also a power law ($n(s) \propto s^{-q}$), with a slope (O'Brien & Greenberg 2003) of

$$q = \frac{7 + b/3}{2 + b/3}. \tag{5}$$

In debris discs, $Q^*_{\rm D}$ scales differently with size for small bodies in the strength regime and for large bodies in the gravity regime (as in Eq. (4), Benz & Asphaug 1999; Stewart & Leinhardt 2009). Hence, we expect bodies in debris disc cascades to have a broken power-law size distribution, with the break at the transition between the strength and the gravity regime. The transition is at the size of the weakest bodies ($s_{\rm w}$), that is, the size where $Q^*_{\rm D}$ is minimised. For a $Q^*_{\rm D}$ law of the form from Eq. (4) the size of the weakest bodies (Wyatt et al. 2011) is given by

$$s_{\rm w} = \left(-\frac{Q_{\rm g} b_{\rm g} s_{\rm g}^{-b_{\rm g}}}{Q_{\rm s} b_{\rm s} s_{\rm s}^{-b_{\rm s}}}\right)^{1/(b_{\rm s}-b_{\rm g})}, \tag{6}$$

where $b_{\rm s} < 0$, making the expression in the parentheses positive. For the dispersal law assumed here, $s_{\rm w} \approx 110$ m. The differential size distribution is given by

$$n(s) = \begin{cases} K_{\rm s} s^{-q_{\rm s}}, & s < s_{\rm w}, \\ K_{\rm g} s^{-q_{\rm g}}, & s > s_{\rm w}, \end{cases} \tag{7}$$

where $q_{\rm s} = 3.66$ and $q_{\rm g} = 3.03$ are the slopes in the strength and the gravity regime, calculated using Eq. (5) and the adopted values for $b_{\rm s}$ and $b_{\rm g}$ from Eq. (4), respectively. The normalisation constant $K_{\rm s}$ for the small bodies is calculated by assuming the observed dust mass ($M_{\rm dust}$) is the mass of particles up to $s_{\rm cm} = 1$ cm,

$$K_{\rm s} = \frac{3(4 - q_{\rm s})}{4\pi\rho_{\rm s}} s_{\rm cm}^{q_{\rm s}-4} M_{\rm dust}. \tag{8}$$

We assume the bulk density of particles is $\rho_{\rm s} = 2.6$ g cm^{-3}. These assumptions are consistent with how our dust masses are obtained from continuum fluxes (Marino et al. 2026a, and see also Sect. 2).

For large bodies, the normalisation constant $K_{\rm g}$ is calculated from a requirement that at steady-state the mass flux through

the cascade is independent of size, and therefore equal in the strength regime and in the gravity regime. Following Wyatt et al. (2011), but accounting for the velocity dependence of $Q_{\rm D}^*$, we find

$$K_{\rm g} = K_{\rm s}\sqrt{\frac{1-q_{\rm g}}{1-q_{\rm s}}}\left[\frac{2}{v_{\rm rel}^2}\left(\frac{v_{\rm rel}}{v_0}\right)^{b_{\rm v}}\right]^{(q_{\rm g}-q_{\rm s})/6}\frac{\left(Q_{\rm s}s_{\rm s}^{-b_{\rm s}}\right)^{(1-q_{\rm s})/6}}{\left(Q_{\rm g}s_{\rm g}^{-b_{\rm g}}\right)^{(1-q_{\rm g})/6}}. \quad (9)$$

The size distribution modelled in this way contains a small discontinuity between the two regimes, whose root cause is the fact that targets just above the transition (sizes just above $s_{\rm w}$) are destroyed by projectiles whose size distribution is that of the small bodies in the strength regime (O'Brien & Greenberg 2003; Wyatt et al. 2011). Nevertheless, similar analytic broken power-law distributions have been shown to agree well with numerical simulations (O'Brien & Greenberg 2003; Löhne et al. 2008; Wyatt et al. 2011). In simulations, and we expect in reality, there is no discontinuity at the transition. Instead, the transition between the strength and the gravity regime causes 'ripples' or 'waves' in the distribution of the large bodies. The amplitude of these waves is similar to the magnitude of the discontinuity in the analytic model. We neglect these waves in this work.

3.4. Fragmentation timescale

The critical projectile-to-target mass ratios calculated above indicate that the estimated collision velocities are sufficiently high for particles to be fragmented. We calculated the timescale on which bodies of different sizes fragment. For this purpose, we used a simple particle-in-a-box collisional model similar to Wyatt et al. (2007) and Wyatt et al. (2011). We assumed all particles are well mixed within the volume of the disc given by

$$V = 4\pi r^2 \Delta r h, \quad (10)$$

where r, Δr and h are the radius of the belt centre, its full width and its aspect ratio, respectively, estimated from observations as described in Sect. 2. Likewise, we assume all particles collide, on average, with the same relative velocity ($v_{\rm rel}$, estimated as described above).

Targets can be destroyed by all projectiles larger than the critical projectile size. The fragmentation rate of a target of size $s_{\rm t}$ is given by

$$R_{\rm frag} = \frac{\pi v_{\rm rel}}{V}\int_{s_{\rm c}}^{s_{\rm max}} n(s_{\rm p})(s_{\rm t}+s_{\rm p})^2 {\rm d}s_{\rm p}, \quad (11)$$

where $s_{\rm max}$ is the radius of the biggest body in the disc. We further assume that $q > 3$ so that small sizes dominate the collisional cross-section (this is true for our steady-state distribution). We also use the fact that the critical projectile sizes we found tend to be much smaller than the target sizes ($s_{\rm c} \ll s_{\rm t}$). Under these assumptions, we have

$$R_{\rm frag} \approx \frac{\pi v_{\rm rel}}{V}\frac{K_{\rm c}s_{\rm c}^{1-q_c}s_{\rm t}^2}{(q_c-1)}, \quad (12)$$

where the size distribution constant, $K_{\rm c}$, and slope, $q_{\rm c}$, depend on the size distribution around $s_{\rm c}$.[1] The fragmentation timescale is simply the inverse of the rate,

$$t_{\rm frag} = \frac{(q_c-1)V}{\pi K_{\rm c} v_{\rm rel}}s_{\rm c}^{q_c-1}s_{\rm t}^{-2}. \quad (13)$$

[1] For a complete solution to the integral without the above assumptions, we refer the reader to Löhne et al. (2008).

We note that in this simple model, the dependence of the fragmentation timescale on the disc scale-height is purely through the critical projectile size, since other occurrences of h get cancelled out.

The results are shown in Fig. 2. We find that the collisional lifetimes of the observed mm-sized grains are several orders of magnitude shorter than the system ages, as expected (since the lines are below unity at mm sizes in the right-hand-side panel). The dust cannot be primordial (i.e. a remnant from the protoplanetary disc phase) and, instead, it has to have been produced more recently (Backman & Paresce 1993). The collisional lifetimes are also at least $\sim$ 100 times longer than the orbital timescale (see Fig. B.1).

We also do not show the lifetime (i.e. we cut off the plotted lines) for large particles for which Eq. (3) evaluates to above unity, as such particles cannot, in fact, be catastrophically disrupted by bodies smaller than themselves. All lines on the right in the right-hand-side panel cross above $t_{\rm frag}/t_{\rm age} = 1$, showing that the limiting factor to particles participating in the cascade is indeed their collisional timescale as opposed to them being too strong to be disrupted.

3.5. Minimum initial disc mass

A disc in a steady-state collisional cascade loses mass over time. Assuming that mass is the only disc property that changes (e.g. the size distribution slope is fixed), disc mass decreases as (Wyatt et al. 2007)

$$M_{\rm disc} = M_0/(1+t/t_0), \quad (14)$$

where M_0 is the initial disc mass and t_0 is the initial fragmentation timescale of the largest bodies. The initial disc mass is unknown, but its minimum value can be constrained (Krivov & Wyatt 2021; Pearce et al. 2025) via

$$M_0 \geq 4|\dot{M}|t_{\rm age}, \quad (15)$$

where $\dot{M}$ is the current mass loss rate through the cascade,

$$\dot{M} = -\frac{M(s_{\rm dust})}{t_{\rm frag}(s_{\rm dust})}, \quad (16)$$

where $M(s_{\rm dust})$ is the mass in particles of size around $s_{\rm dust}$. Here and throughout this work, we estimate the mass in particles of size around some size s as the mass in the unit log-bin of size around s,

$$M(s) = \frac{4\pi\rho_s}{3}Ks^{4-q}, \quad (17)$$

where K and q are the normalisation and the slope of the size distribution around s. Using the ARKS dataset, the steady-state size distributions and the fragmentation timescales calculated as outlined in previous sections, adopting $s_{\rm dust} = 1$ mm, we find minimum initial disc masses in the range of $0.1 - 200\,{\rm M}_\oplus$. This is only a rough, order-of-magnitude estimate, as the chosen width of the size bin in $M(s)$ is arbitrary. Had we chosen to define $M(s)$ as the mass from μm-sized to mm-sized grains, the inferred masses would be larger by a factor of ~ 7. The choice of $s_{\rm dust}$ is also arbitrary, but it is irrelevant – by definition our steady-state collisional cascade model has a mass flow rate that is constant

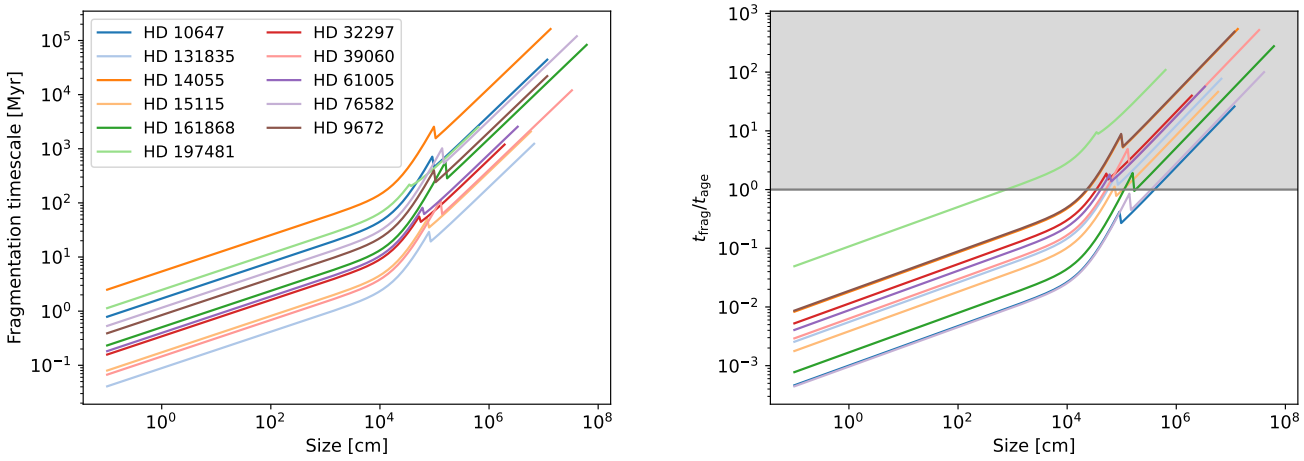


Fig. 2. *Left*: Fragmentation timescale as function of particle size. *Right*: Ratio of the fragmentation timescale and the system age for each of the discs. Lines on the right follow the same key legend shown in the panel on the left. Lines are cut off at the upper end at the sizes at which the critical disruption energy becomes too large and the bodies cannot be catastrophically disrupted except in collisions with larger bodies. In the right-hand-side panel, the gray region shows where the fragmentation timescale is longer than system age.

with size. An alternative is to consider small, blowout-sized particles, which are assumed to dominate the discs' fractional luminosities (f) with a mass-loss rate (Matrà et al. 2017) given by

$$\dot{M} = -\frac{M_{\rm blowout}}{t_{\rm frag}(s_{\rm blowout})} \tag{18}$$

$$= -1.2\times10^{3}\,\frac{\mathrm{M}_\oplus}{\mathrm{Myr}}\left(\frac{r}{\mathrm{au}}\right)^{3/2}\left(\frac{\Delta r}{\mathrm{au}}\right)^{-1} f^2\,\frac{L_*}{\mathrm{L}_\odot}\left(\frac{M_*}{\mathrm{M}_\odot}\right)^{-1/2}. \tag{19}$$

The expression follows from the same collisional model employed in this work (Wyatt et al. 2007). Matrà et al. (2017) assume a size distribution slope $q = 3.5$, different from our $q_{\rm s} = 3.66$, but this would change the mass-loss rate only by about a percent (see their Eq. 19). For the blowout-sized particles, there is no dependence on the collision velocity (or on the disc's aspect ratio) because the critical projectile-target size ratio is irrelevant – smaller particles are blown out by radiation pressure and blowout-sized particles predominantly collide with equal-sized particles.

Minimum initial disc masses estimated from fractional luminosities tend to be somewhat lower than the masses estimated from millimetre dust masses, as shown in Fig. 3. Nevertheless, the two estimates largely agree within an order of magnitude. This is striking in view of the vast simplifications made to relate the measured fractional luminosities with the number and the location of blowout-sized grains and any contribution from sub-blowout grains, and to estimate the mass flow rate at millimetre sizes. The agreement between the two estimates is good even for HD 197481 (AU Mic) and HD 61005, two low-luminosity stars for which the minimum dust grain size may very likely not be the blowout limit set by radiation pressure, and this points to the need for caution when interpreting these agreements.

3.6. Initial disc mass and planetesimal size

Further constraints on the bodies hiding in the disc can be achieved, albeit with some additional assumptions. In this section we extrapolate the size distribution of larger bodies from the observed dust masses assuming steady-state collisional cascades (see Sect. 3.3) and we estimate the sizes at the upper end of the cascades, that is, sizes of the planetesimals feeding the cascades.

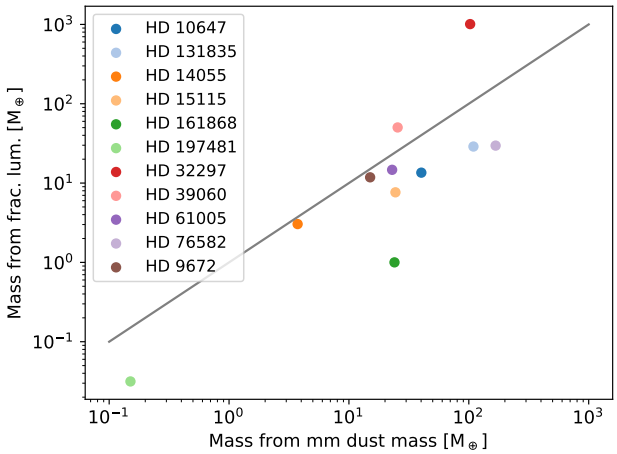


Fig. 3. Minimum initial mass in collisional cascade calculated using millimetre dust mass compared to mass calculated using fractional luminosity. Gray line indicates where the two are equal.

First, we note that the minimum initial disc mass from Eq. (15) corresponds to the initial fragmentation timescale of the largest bodies being equal to the system age (this follows simply from minimisation of the initial disc mass over the initial fragmentation timescale; Pearce et al. 2025). Indeed, there are strong arguments to assume that the planetesimals at the top of a steady-state cascade, of radius $s_{\rm pl}$, are those whose fragmentation timescale equals the system age, and they represent the lower limit on the size of primordial bodies in the disc (Wyatt & Dent 2002). Primordial planetesimals in an observed disc cannot be much smaller because smaller planetesimals fragment too quickly and any initial disc mass would have been depleted by the estimated age of the systems[2]. On the other hand, larger plan-

[2] This can also be verified by expressing the initial disc mass required to explain the current dust mass with largest planetesimals of some size, $s < s_{\rm pl}$, in terms of the initial disc mass required for $s = s_{\rm pl}$, using Eqs. (14), (17) and (13). Smaller planetesimals require larger initial disc masses to explain dust detections. As first noted by Wyatt & Dent

etesimals may exist in each disc, but in the steady-state model their collisions are happening too infrequently to have produced a lot of dust, and they still have their primordial distribution (Löhne et al. 2008). Such larger bodies may contribute to the cascade through non-disruptive, erosive collisions, and this possibility is explored in a companion paper by Chiang et al. (2026).

Second, we recall that the relevant fragmentation timescale is that at the start of the cascade, that is, at time $t = 0$. As already noted above, the fragmentation timescale at the start is a function of the initial disc mass. Additionally, the initial size distribution may differ from the one at steady-state (Löhne et al. 2008; Schlichting et al. 2013; Krivov et al. 2018; Krivov & Wyatt 2021). Here, we follow Löhne et al. (2008) and Krivov & Wyatt (2021) and assume that the size distribution of primordial planetesimals was a power law characterised by q_p and K_p. The initial disc mass obtained from this analysis will therefore differ from the one obtained in the previous section, where the underlying assumption of Eq. (14) is that the size distribution is fixed to the steady-state distribution from the start.

We find the size of planetesimals feeding a cascade by requiring that $t_\mathrm{frag}(s_\mathrm{pl}) = t_\mathrm{age}$ and that the mass in these planetesimals, $M(s_\mathrm{pl})$, equals the current, steady-state mass in these bodies (see also Sect. 4.3 of Pearce et al. 2025). For each disc, we calculate the present-day, steady-state size distribution, as described in Sect. 3.3. For an arbitrary planetesimal size, s, we can then calculate the present-day mass in a unit log-bin of size using Eq. (17). We assume that this mass has not changed significantly since $t = 0$, and for a given q_p we can calculate the primordial size distribution normalisation constant K_p. Then, we can calculate the fragmentation timescale of these particles at $t = 0$. The calculation of this fragmentation timescale is analogous to the calculation of the present-day fragmentation timescale presented in Sect. 3.4, except that here we assume $K_\mathrm{c} = K_\mathrm{p}$ and $q_\mathrm{c} = q_\mathrm{p}$ in Eq. (13). We assume the other disc properties were otherwise the same in the past, that is, the spatial distribution of the planetesimals has remained unchanged over the stellar lifetime. Finally, we iteratively solve for the size, $s = s_\mathrm{pl}$, for which $t_\mathrm{frag}(s) = t_\mathrm{age}$.

The resulting planetesimal sizes and the masses contained in these planetesimals are shown in Fig. 4 for $q_\mathrm{p} = 3$ (circles) and $q_\mathrm{p} = 4$ (squares). Overall, the planetesimal sizes range from a few metres to ten kilometres, and the total masses of these planetesimals are less than $200\,\mathrm{M}_\oplus$. If we assumed the primordial size distribution was the same as the present-day steady-state size distribution, the inferred planetesimal sizes would be those for which $t_\mathrm{frag}(s) = t_\mathrm{age}$ in the right-hand panel of Fig. 2, and their values would fall between the two estimates shown in Fig. 4 (because $3 < q_\mathrm{s}, q_\mathrm{g} < 4$).

From these s_pl and q_p values for each disc, we were also able to extrapolate the hypothetical primordial size distributions up to 200 km, shown as the lines in Fig. 4. These large planetesimal sizes are predicted by planetesimal formation models (Johansen et al. 2015; Simon et al. 2016; Schäfer et al. 2017), but their existence is not required to explain the observations (because their $t_\mathrm{frag}(s) > t_\mathrm{age}$; Krivov & Wyatt 2021).

In contrast, our assumed primordial size distributions require some planetesimals smaller than s_pl to be initially present. The primordial power-law distributions are assumed to extend down to at least the critical projectile size for s_pl, and the critical projectile sizes are about 2 to 20 times smaller than s_pl.

(2002), for s that is only moderately lower than s_pl (e.g. for $s = s_\mathrm{pl}/4$ in the idealised cascade with $Q^*_\mathrm{D} = \mathrm{const}$ and $q = 3.5$), the required initial disc mass becomes infinite.

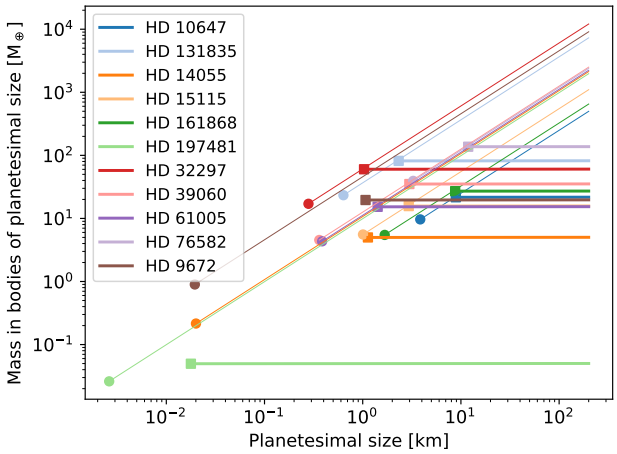


Fig. 4. Planetesimal sizes feeding the cascades assuming primordial power-law size distribution with slope $q_\mathrm{p} = 3$ (circles) and its extrapolation up to 200 km (thin lines), and likewise for $q_\mathrm{p} = 4$ (squares and thick lines), plotted against the corresponding mass inside unit log bin of size around the planetesimal size. For a size distribution with slope $q_\mathrm{p} = 4$ there is equal mass in each log bin of size.

If such smaller sizes do not exist at $t = 0$, or their number is smaller than implied by these power laws, the initial fragmentation timescales would be longer and the planetesimals feeding the cascade would need to be smaller than values of s_pl shown in Fig. 4. For example, consider the extreme case of an initial size distribution that is a Dirac delta function centred at the parent planetesimal size. We can solve for this planetesimal size in a manner similar to above, and this yields particle radii of only 10 cm – 10 m.

Putting this caveat aside, we explored the relationship between our inferred planetesimal sizes shown in Fig. 4 and stellar masses and disc radii, the two quantities we have in our dataset, which could influence the initial planetesimal mass function (e.g. Gerbig & Li 2023). We did not find any correlations.

4. Constraints on stirrers

In this section, we present the constraints we set on the sizes and surface densities of large bodies whose gravitational interactions with planetesimals and dust could result in the observed disc scale-heights. We assume that: (1) stirrers are embedded within the disc; (2) stirrers fully formed early on, during the protoplanetary disc stage or quickly after; (3) planetesimals and dust have been stirred starting from a negligibly low excitation level, for the duration of the system's lifetime; and (4) excitation of stirrers is at all times lower than that of planetesimals and dust. We discuss these assumptions and alternative theories in Sects. 5.2.4 and 5.3.

If a disc starts with a very low excitation, the gravitational interactions with embedded stirrer(s) initially occur in a shear-dominated (or sub-Hill) regime where relative velocities are primarily determined by Keplerian shear. This is up until particle eccentricities increase sufficiently to drive higher relative velocities, and the disc enters the dispersion-dominated (or super-Hill) regime. Debris discs are typically assumed to be in the dispersion-dominated regime (e.g. Quillen et al. 2007; Pan & Schlichting 2012; Matrà et al. 2019), and so we first present results making the same assumption. We then verify that none

of the discs in our sample are currently in the shear-dominated regime if collisional damping is neglected, and finally we consider the role of collisional damping.

4.1. Gravitational stirring in dispersion-dominated regime

To constrain properties of the stirrers in the dispersion-dominated regime, we largely follow the approach of Matrà et al. (2019). As in their work, we use the semi-analytic stirring rates from Eqs. (4.1) and (4.2) from Ida & Makino (1993) to determine the time evolution of particle eccentricities and inclinations. For details, see Appendix C. Given the system age and present-day inclination dispersion, the product of stirrer mass, $M_{\rm stir}$, and surface mass density, $\Sigma_{\rm stir}$, of stirrers can be expressed as

$$M_{\rm stir}\Sigma_{\rm stir} = 0.25 G^{-1/2} M_*^{3/2} r^{-1/2} t_{\rm age}^{-1} i_{\rm rms}^4, \tag{20}$$

where G is the gravitational constant and $i_{\rm rms} = \sqrt{\langle i^2 \rangle} = \sqrt{2}h$ is the root mean square of the particle inclinations. This formula is approximately valid in the case of a large number of small stirrers, as well as for a single stirrer with an effective surface density determined by the stirrer's mass and the width of the zone in which its stirring is effective (stirring width; Ida & Makino 1993), up to a factor of an order of unity, which depends on whether the bodies are stirring themselves or whether they are stirred by a larger body or bodies.

There needs to be at least one whole stirrer within the disc and within its own stirring width, and so there is a minimum (effective) surface density,

$$\Sigma_{\rm stir} > \frac{M_{\rm stir}}{2\pi r \min(\Delta r, \Delta r_{\rm stir})}, \tag{21}$$

where $\Delta r_{\rm stir} \approx 4 r h_{\rm Hill} \sqrt{12 + 20/3 (i_{\rm rms}/h_{\rm Hill})^2}$ is the stirring width (Ida & Makino 1993) and

$$h_{\rm Hill} = \left(\frac{M_{\rm stir}}{3 M_*} \right)^{1/3} \tag{22}$$

is the reduced Hill radius.

Furthermore, for a fixed size of the stirrer(s), there is a maximum excitation that can be achieved, corresponding to $v_{\rm rel} \sim v_{\rm esc} = \sqrt{2GM_{\rm stir}/R_{\rm stir}}$, the escape velocity of the stirrer(s) (Safronov 1972; Goldreich et al. 2004; Schlichting 2014), where $R_{\rm stir}$ is the stirrer radius. For higher relative velocities gravitational focusing becomes inefficient. Particles are then more likely to physically collide with the stirrer than they are to gravitationally scatter. This yields a constraint on the minimum mass of the largest bodies in the disc (e.g. Matrà et al. 2019; Marino 2021; Terrill et al. 2023), expressed as

$$M_{\rm stir} > 2.5 \rho_{\rm stir}^{-1/2} M_*^{3/2} r^{-3/2} i_{\rm rms}^3. \tag{23}$$

For the stirrers, we assumed $\rho_{\rm stir} = 2\,{\rm g\,cm^{-3}}$, noting that we find stirrers' sizes range from minor bodies to Neptune-sized planets, so their bulk density might be diverse in reality. We added another constraint: the total mass of stirrers in the belt implied by $\Sigma_{\rm stir}$ cannot be larger than the solid mass contained inside the systems' protoplanetary discs, $M_{\rm PPD}$. This gives

$$2\pi r \Delta r \Sigma_{\rm stir} < M_{\rm PPD}. \tag{24}$$

Here, we assume the spatial distribution of stirrers has not evolved over the system's lifetime and it is similar to the spatial distribution of dust. We can estimate $M_{\rm PPD}$ using the standard dust-to-gas ratio of 0.01 and a total PPD mass of 0.1 of the stellar mass (Williams & Cieza 2011). We used the solid mass because the stirrers we found are mostly smaller than $20\,{\rm M_\oplus}$, corresponding to sub-Neptunes, which are expected to have less than a few percent of their mass in their atmospheres.

Together, the four constraints in Eqs. (20), (21), (23), and (24) yield finite ranges of $M_{\rm stir}$ and $\Sigma_{\rm stir}$ shown in the left panel of Fig. 5. There is a wide dispersion in the mass of stirrers inferred, from planetesimal-sized bodies for HD 197481 (but see Sect. 4.3) to several tens of Earth mass for HD 39060 and HD 161868. Overall, these masses are realistic, such a wide range of large bodies may indeed exist in different planetary systems, albeit this raises the question of what planet formation processes create the dispersion. Furthermore, we find that Eq. (23) should be used with caution. For all discs except for HD 197481 we find that the condition on the maximum disc mass from Eq. (24) is more stringent than the lower limit on stirrers' individual masses from Eq. (23). This means that for almost all discs in the sample the smallest possible stirrers from Eq. (23) need to be unrealistically numerous, with their total mass larger than the mass available in the solids in their nascent protoplanetary disc to stir the discs within system age.

4.2. Gravitational stirring in shear-dominated regime

A similar semi-analytic model describes stirring in the shear-dominated regime (Eq. 4.7 in Ida & Makino 1993), with a corresponding constraint,

$$M_{\rm stir}^{-1/3}\Sigma_{\rm stir} \approx G^{-1/2} M_*^{1/6} t_{\rm age}^{-1} r^{-1/2} \ln \frac{i_{\rm rms}}{i_0}, \tag{25}$$

where i_0 is the initial inclination of particles. For details, see Appendix C. We assume that $i_0 = 10^{-4}$ and note that the dependence of our results on it is only logarithmic. Reducing i_0 by several orders of magnitude only makes $M_{\rm stir}^{-1/3}\Sigma_{\rm stir}$ increase by a factor of a few.

The minimum surface density given by Eq. (21) that applies here is same as in the dispersion-limited regime. However, the minimum mass of the stirrers is different. For the disc to be in the shear-dominated regime, $i_{\rm rms} \lesssim h_{\rm Hill}$. From Eq. (22) it follows that

$$M_{\rm stir} > 3 M_* i_{\rm rms}^3. \tag{26}$$

This is equivalent to the requirement that the velocity dispersion is not larger than the Hill velocity, whereas in the dispersion-dominated regime the requirement is that it cannot be larger than the escape velocity of the stirrers.

We find that there are no combinations of $\Sigma_{\rm stir}$ and $M_{\rm stir}$ for which all three of the conditions given by Eqs. (21), (25), and (26) are satisfied, for any of the discs in our sample. We illustrate this by showing the constraints for the disc with the lowest aspect ratio in Fig. 6. The red line shows the constraint from Eq. (25). Along this line, either the mass of individual stirrers is too low to be consistent with the shear-dominated regime at the given excitation, or the surface density is too low for the stirring width to contain one whole stirrer. We conclude that none of our discs are in the shear-dominated regime.

We can also test if neglecting the brief shear-dominated phase affects our results in the dispersion-dominated regime. We can calculate $t_{\rm Hill}$, the time it takes to stir $i_{\rm rms}$ to $h_{\rm Hill}$. The constraint ΣM calculated in the previous section should change by a factor $\sim (t_{\rm age} - t_{\rm Hill})^{-1}(i_{\rm rms}^4 - h_{\rm Hill}^4)/(t_{\rm age}^{-1} i_{\rm rms}^4)$. We find that $t_{\rm Hill}/t_{\rm age}$

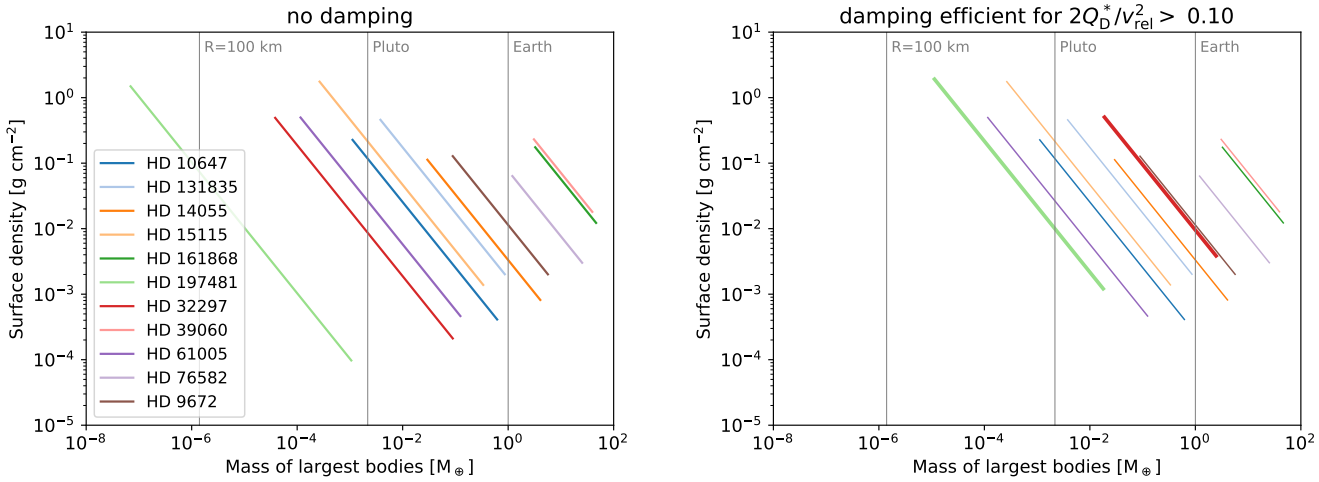


Fig. 5. Constraints on the surface density of stirrers as function of their mass, assuming stirring in dispersion-dominated regime. Left: No collisional damping. The product of the surface density and the mass is constrained by the stirring timescale and given by Eq. (20). The lines indicate the corresponding possible combinations of stirrers' surface density and mass. The endpoints of lines are determined by the minimum and the maximum surface density, and the minimum mass, given by Eqs. (21), (24) and (23), respectively. Right: Stirring is balanced by collisional damping if damping is faster than fragmentation, in which case the constraints are obtained by equating the stirring rate with the damping rate from Eq. (27). Damping is efficient in only two discs (HD 197481 and HD 32297), shown by the thick lines.

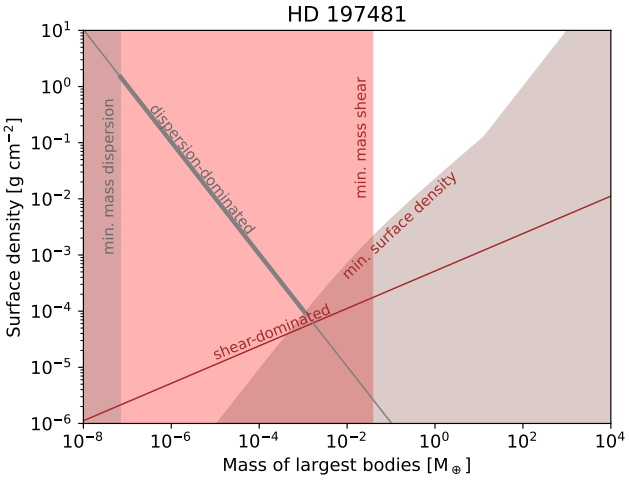


Fig. 6. Constraints on surface density and mass of stirrers assuming stirring in the dispersion-dominated regime compared to the shear-dominated regime for HD 197481, ignoring collisional damping. The gray line for the dispersion-dominated regime is determined by Eq. (20) and the red line for the shear-dominated regime by Eq. (25). The minimum surface density condition given by Eq. (21) applies to both regimes. In the shear-dominated regime, the minimum mass is determined by the condition that the stirring is indeed in this regime, given by Eq. (26). For this disc, when damping is neglected, the left endpoint for the dispersion-dominated regime is determined by the minimum mass from Eq. (23), but note the condition on the maximum surface density from Eq. (24) is more stringent for most discs.

is less than a percent and $i_{\rm rms}/h_{\rm Hill}$ at least a few, making this factor very close to unity for all discs in our sample.

A caveat to these findings is that gravitational scattering at low relative velocities is more complex than in the dispersion-regime (see the discussion in Sect. 4.3 of Goldreich et al. 2004). The semi-analytic approach is less accurate in the shear-dominated regime than in the dispersion-dominated regime, when compared with numerical simulations (Ida & Makino 1992; Stewart & Ida 2000).

4.3. Collisional damping

Gravitational stirring might be balanced by collisional damping (Brahic 1977; Hornung et al. 1985; Pan & Schlichting 2012), a process in which the loss of kinetic energy in inelastic collisions tends to reduce the velocity dispersion (and thus the eccentricity and the inclination dispersion) of dust and/or planetesimals. The damping rate for hard, indestructible targets of size $s_{\rm t}$ can be estimated (Hornung et al. 1985; Jankovic et al. 2024) as

$$R_{\rm damp} = \frac{\pi v_{\rm rel}}{V} \int_{s_{\rm min}}^{s_{\rm max}} n(s_{\rm p})(s_{\rm t}+s_{\rm p})^2 \frac{2 s_{\rm t}^3 s_{\rm p}^3}{(s_{\rm t}^3+s_{\rm p}^3)^2} {\rm d}s_{\rm p} \quad (27)$$

$$\approx \frac{\pi v_{\rm rel}}{V} 2 K_{\rm t} s_{\rm t}^{3-q_{\rm t}}, \quad (28)$$

where $K_{\rm t}$ and $q_{\rm t}$ are the normalisation and the exponent of the size distribution near $s_{\rm t}$. The approximation holds for power laws with an exponent of $q < 4$, for which large bodies contain most of the mass. The expression is equivalent to Eq. 12 from Pan & Schlichting (2012).

To revise our constraints on $\Sigma_{\rm stir} M_{\rm stir}$ of stirrers in the dispersion-dominated regime, we can derive an equation analogous to Eq. (20) by equating the stirring rate to the collisional damping rate (Pan & Schlichting 2012), for a dust size that contributes most to the observed flux at millimetre wavelengths, $s_{\rm t} = 1$ mm. However, damping has to act within the collisional lifetime of dust particles. Dust particles are part of the collisional cascade, continually produced in collisions of larger particles and continually destroyed in collisions with smaller ones. Damping is most efficient in collisions with equal-sized particles. If particles collide with and get disrupted by smaller particles much more frequently than they collide with equal-sized particles, collisional lifetime is shorter than the damping timescale, and damping is overall inefficient (Jankovic et al. 2024).

Therefore, to revise our constraints on $\Sigma_{\rm stir} M_{\rm stir}$ of stirrers, we require that $t_{\rm damp} < t_{\rm frag}$, where $t_{\rm damp} = 1/R_{\rm damp}$. Assuming

$K_c = K_t$ and $q_c = q_t = q$, the ratio of the timescales is given by

$$\frac{t_{\rm frag}}{t_{\rm damp}} = 2(q-1)\left(\frac{2Q_{\rm D}^*}{v_{\rm rel}^2}\right)^{(q-1)/3}. \quad (29)$$

In the strength regime relevant for the dust ($q = q_s = 3.66$), the damping timescale is shorter than the fragmentation timescale if the critical projectile-to-target mass ratio $2Q_{\rm D}^*/v_{\rm rel}^2 \gtrsim 0.1$. We verify this by also numerically integrating Eqs. (27) and (12). Only two of our discs fulfil this condition (HD 197481 and HD 32297). For these two discs we replace the constraints on $\Sigma_{\rm stir}M_{\rm stir}$ from Eq. (20) with an analogous expression derived from equating the stirring and the damping rate. We show the results in the right-hand-side panel of Fig. 5, in which these two discs are shown with thick lines.

In these calculations, we assumed that collisional damping acts on the observable dust particles. The critical specific energy for fragmentation, $Q_{\rm D}^*$, is a non-monotonic function of size (see Fig. 1), and so it may occur that collisions among dust grains are not damping, but that collisions among their parent bodies are. For the discs in our sample, this is not the case. Assuming the parent bodies are those bodies whose fragmentation timescale is equal to the system age (i.e. for the planetesimals feeding the cascades, whose properties we constrained in Sect. 3), we numerically calculated their collisional damping timescales for $q_p = 3$ and $q_p = 4$ and found them to be longer than the system age for each disc.

Fragmenting collisions among the parent bodies may contribute to their velocity evolution and thus influence the stirrer properties constrained here. Models that consider the full velocity distribution, rather than only a characteristic collision velocity, show that fragmentation depends non-trivially on the orbital element distributions of both targets and projectiles, potentially affecting the velocity dispersion (Jankovic et al. 2024). However, these models predict only slow evolution of the average particle inclination, and further work is required to distil their results into prescriptions suitable for constraining disc parameters in simple models such as ours.

Dynamical friction also cannot damp parent bodies' velocities. The inferred collision velocities are higher than the escape velocity of bodies in the cascade for each of the discs. Therefore, the rate of cooling by dynamical friction is equal to the rate of collisional damping (Goldreich et al. 2004; Pan & Schlichting 2012), and the same conclusions apply as above.

We also checked how collisional damping changes our conclusions so far for the shear-dominated regime. We derive an equation analogous to Eq. (25) by equating the stirring rate from Ida & Makino (1993) with the collisional damping rate, and we apply the new constraints on $\Sigma_{\rm stir}$ and $M_{\rm stir}$ for the two discs in which collisional damping may be acting. We find that only HD 32297 could be stirred in the shear-dominated regime (the red line in Fig. 6 moves up into the allowed white region for this disc). The possible masses of the stirrers range from ~ 3 to $10\,M_\oplus$.

In summary, with a simple prescription for the efficiency of collisional damping, we find that velocity damping from mutual collisions of dust grains balances out gravitational stirring in only two of the eleven discs in our sample (HD 197481 and HD 32297). Taking this into account results in new constraints on the properties of stirrers for these two discs, as shown in the right-hand-side panel of Fig. 5. The total dispersion in the masses of stirrers in the sample is reduced compared to the damping-free calculations in Sect. 4.1, but still significant. The stirring occurs in the dispersion-dominated regime for all of the discs, except, possibly, for HD 32297.

5. Discussion

5.1. Debris disc inventories and masses

5.1.1. Planetesimals

Our collisional modelling shows that the debris discs in our sample contain primordial planetesimals with minimum sizes ranging from ~ 10 m to 10 km and minimum masses of $\sim 10^{-2}$ to $10^2\,M_\oplus$ (see Figs. 3 and 4). These bodies feed the presumed steady-state collisional cascades producing the observed dust. Six of our discs (HD 9672, HD 15115, HD 39060, HD 61005, HD 131835, and HD 197481) were previously modelled by Krivov & Wyatt (2021). Despite differences in the modelling and adopted disc properties, our minimum disc masses agree well with theirs for four systems. For HD 9672 and HD 197481 our masses are about an order of magnitude smaller.

HD 197481 (AU Mic) seems to be an outlier in general. Its very low planetesimal and stirrers' mass appears to be driven by its extremely low aspect ratio. It should be noted, however, that the minimum disc mass we derive from fractional luminosity is independent of the aspect ratio, and it is even smaller than the one we derive from millimetre dust mass, and also consistent with a previous estimate of collisional mass of $\sim 0.01\,M_\oplus$ from Strubbe & Chiang (2006). A stochastic catastrophic disruption event has previously been proposed (Chiang & Fung 2017) as an explanation for time-variable features observed in this disc at short wavelengths (Boccaletti et al. 2015). This offers an alternative explanation for this system's unusual properties.

As in Krivov & Wyatt (2021), we find that the planetesimals feeding the cascades have total masses smaller than $\sim 100\,M_\oplus$. Extrapolating the primordial size distribution up to 200 km with a relatively flat size distribution leads to unrealistically large disc masses, over $1000\,M_\oplus$, an issue known as the 'debris disc mass problem' (Krivov & Wyatt 2021).

Recently, Marshall et al. (2026a) found extrapolated disc masses that are smaller than $1000\,M_\oplus$ for all 11 discs in our sample. The difference from our work seems to come mainly from the dust masses in their work being about 10 times smaller, which can partly be explained by different assumptions about the dust size distribution and composition.

5.1.2. Stirrers

Our results show that minimum-mass stirrers defined by Eq. (23) would need to have a total mass larger than the solid mass of their primordial protoplanetary disc for all but one disc. This stands in contrast to findings of Zawadzki et al. (2026), who find all but three of the discs could have been stirred by these bodies with reasonable disc masses. The difference comes from that in the definition of the stirring timescale. To calculate the stirring timescale (but not for the rest of their calculations), Zawadzki et al. (2026) employed the model of Krivov & Booth (2018) which only considers if a disc can be stirred sufficiently for bodies to start disrupting, that is, up to a critical fragmentation velocity of $30\,{\rm m\,s^{-1}}$. In this work, we consider if bodies are stirred up to an average relative velocity implied by the observed aspect ratios, which we find to be in the range of $40\,{\rm m\,s^{-1}}$ to $2600\,{\rm m\,s^{-1}}$.

The sizes of the stirrers we infer mostly range from the size of Pluto to sub-Neptunes. This implies that most discs cannot be

stirred to their observed aspect ratios by the 200 km-sized planetesimals expected from planetesimal formation theory, although stirring by those planetesimals would be strong enough to trigger the collisional cascade (Krivov & Booth 2018). However, the stirrers being large does not necessarily mean that the stirrers have been accreting material beyond the protoplanetary disc phase, or that delayed stirring (Kenyon & Bromley 2002, 2004, 2008, 2010) has occurred. The stirrers could also have formed early on, inside the protoplanetary disc, consistent with our assumptions. Analyses of the structure of observed protoplanetary discs suggest that sub-Neptunes already exist early on at the orbital distances of 10s of au, comparable to debris disc sizes, albeit from theoretical arguments it appears challenging to prevent their inward migration and keep them at large orbital separations (e.g. Lodato et al. 2019).

5.1.3. Connection between planetesimals and stirrers

In Fig. 7, we show the full inventories of the debris discs modelled in this work. For the stirrers we convert the surface density constraints into their total mass within each disc, $\Sigma_{\rm stir} 2\pi r \Delta r$. Recall that for the stirrers we constrain the product of their surface density and their mass – stirrers' total (and individual) masses may lie anywhere along the lines shown in Fig. 7.

We find that stirrers do not necessarily contain most of the mass within a disc – for some discs a part of the line (showing possible stirrers' total mass) in Fig. 7 falls below the circles/squares (showing possible planetesimals' total mass). This is analogous to how Zawadzki et al. (2026) find that some of their stirring disc masses are less than the collisional disc masses inferred by Krivov & Wyatt (2021). Similarly, Pearce et al. (2025) find that the narrow belt of Fomalhaut may contain Pluto-sized stirrers, but if so their total mass could only be only a small fraction of the belt's mass, or otherwise gravitational scattering would make the belt radially broader than it is. Such combinations of stirring and collisional constraints are fully valid: for bodies to dominate stirring it is the product $\Sigma_{\rm stir} M_{\rm stir}$ that needs to be larger, rather than just the total surface density or total mass (Ida & Makino 1993; Quillen et al. 2007; Krivov & Booth 2018).

Throughout this work, we assume that the planetesimals and the stirrers are two distinct populations, with planetesimals feeding the collisional cascades and stirrers providing dynamical excitation. Figure 7 is consistent with this assumption, and indeed the relatively small planetesimals cannot produce the observed disc aspect ratios. However, a companion paper by Chiang et al. (2026) shows that stirrers might in fact contribute to the collisional cascade through erosive, non-disruptive collisions. Naturally, for this to occur, the stirrers' total mass needs to be higher than that in the collisional cascade.

In our modelling, we did not assume that a particular distribution extends from planetesimal sizes up to stirrers' sizes. If we go on to assume a posteriori that these bodies are connected by a power law, we can extract the possible ranges for the slopes from Fig. 7. We show these in Fig. 8 as a function of stellar mass. The minimum values are determined by connecting our solutions for planetesimal sizes for $q_{\rm p} = 3$ with the smallest possible stirrers; the latter are mostly determined by setting an upper limit on the total mass in stirrers to be less than the expected solid mass in protoplanetary discs. The maximum values connect our $q_{\rm p} = 4$ solutions to the largest possible stirrers. The maximum values of these inferred primordial slopes may exhibit a weak decreasing trend towards more massive stars (with the exception of the notable outlier HD 197481, see the discussion in Sect. 5.1.1). This might be partly explained by the dependence of our minimum surface density of stirrers on stellar mass through Eqs. (21) and (22).

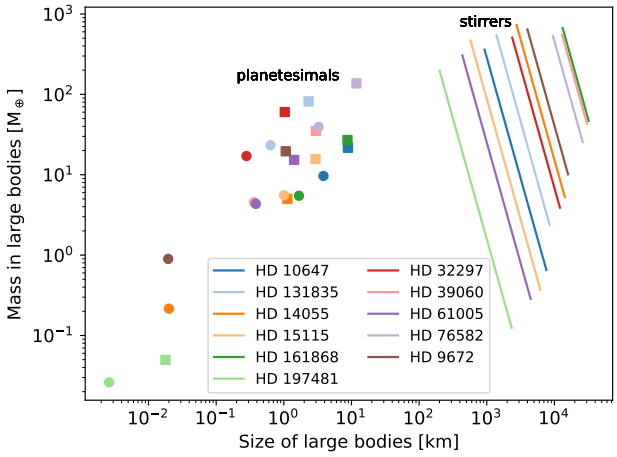


Fig. 7. Joint constraints on sizes of planetesimals feeding the collisional cascades (circles for $q_{\rm p} = 3$ and squares for $q_{\rm p} = 4$, the same as in Fig. 4) and on the stirrers exciting particles' inclinations (solid lines). The constraints on the stirrers show plausible combinations of their total mass and their individual size, and not a size distribution. These constraints account for collisional damping of mm-sized dust in discs in which it is estimated to be efficient.

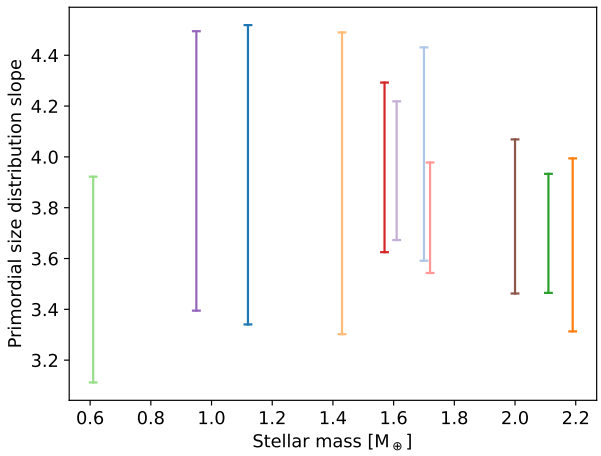


Fig. 8. Primordial size distribution slope ranges for hypothetical power laws connecting constraints on planetesimals and constraints on stirrers. Upper limits are set by extrapolation of planetesimal sizes to sizes of largest possible stirrers, and vice versa for lower limits.

The connection between the planetesimals feeding the cascades and any hypothetical larger bodies is influenced by several planet formation processes. Planetesimal formation via the streaming instabilities and subsequent gravitational collapse is predicted to result in a fairly flat power-law distribution of planetesimals, with an exponential cut-off at larger sizes (Johansen et al. 2015; Simon et al. 2016; Schäfer et al. 2017). Subsequent planetesimal-planetesimal collisions and accretion of pebbles flattens the cut-off (Johansen et al. 2015). Since extrapolating our collisional cascade planetesimals up to the sizes predicted by these studies leads to the disc mass problem (see Sects. 3.6 and 5.1.1, and Krivov & Wyatt 2021), we refrain from making more detailed comparisons to planet formation theory.

5.2. Uncertainties

In this section, we discuss uncertainties within the paradigm we adopted, in which planetesimals feed the steady-state production of the observed dust, while a population of bodies embedded within the discs gravitationally stirs the discs. Further below we discuss alternatives to this paradigm.

5.2.1. Observational uncertainties

First and foremost, our results are likely affected by the selection of targets for the ARKS programme, and may not be representative of all debris discs. ARKS discs are some of the brightest and consequently also some of the youngest among the general population (Marino et al. 2026a).

The uncertainties in the ARKS disc aspect ratio fits estimated by the fitting methods are relatively low (Zawadzki et al. 2026). However, fits with different methods or assuming different vertical profile shapes often yield strikingly different aspect ratios. The extreme example is HD 197481. Assuming Gaussian vertical density distribution yields $h = 0.023$ and $h = 0.026$ with non-parametric methods, which are close to previous estimates (e.g. Daley et al. 2019). Assuming Lorentzian distribution yields $h = 0.0028$ (the value adopted in this work; see Fig. 2 in Zawadzki et al. 2026). A factor of ten difference in h translates to an order-of-magnitude difference in the collisional disc mass and four orders of magnitude in $\Sigma_{\rm stir}M_{\rm stir}$ of stirrers. Besides, Zawadzki et al. (2026) assume that the disc aspect ratio is fixed throughout the disc, whereas at least in some discs it might vary with radius (Matrà et al. 2019; Han et al. 2025).

For our collisional modelling, one key quantity is used implicitly: the dust surface density. We estimated it using the dust masses, radii, and widths from simple Gaussian modelling of the ARKS observations from Marino et al. (2026a), $\Sigma_{\rm dust} = M_{\rm dust}/(2\pi r\Delta r)$. A much more detailed analysis of ARKS discs' radial structures is presented by Han et al. (2026a), including deprojected, deconvolved radial profiles of dust surface density. Our more approximate estimates of dust surface densities agree with the peak dust surface densities in their Fig. 3 remarkably well, with only three exceptions: HD 32297, HD 61005, and HD 131835. These are the discs with narrow peaks imposed on radially extended discs. Even for these three discs, the peak surface density from detailed modelling is less than a factor of 2 or 3 larger than in our modelling. Therefore, our modelling should be accurate for the regions of peak density inside these discs. Radial variations in the surface density and other quantities could be used to uncover radial variations in properties of planetesimals and stirrers, especially for radially wide discs (e.g. HD 14055). However, we refrained from expanding our analysis in this direction because a key quantity – the aspect ratio – was constrained assuming it to be radially constant and possibly only representative of the peak-density region.

Another large source of uncertainty is the system ages. We assumed that the ages of the collisional cascades and the timescale of stirring are equal to the stellar ages compiled from literature by Matrà et al. (2025) and Marino et al. (2026a). Estimates of stellar ages can be affected by systematic errors (e.g. Guzman et al. 2026). The values in literature vary for some discs, for example, from 15 Myr (Rodigas et al. 2014) to 30 Myr (Kalas 2005) for HD 32297 (we assume 30 Myr). Additionally, the relation of the stellar evolution 'zero time' to the disc evolution 'zero time' is highly uncertain. The zero time for pre-main sequence stellar evolution is also difficult to define: the transition from a collapsing protostar to a visible pre-main sequence star is a continuous, gradual process rather than a single, distinct event. Halving the system age would halve the collisional disc mass in planetesimals and double the constraint on stirrers, $\Sigma_{\rm stir}M_{\rm stir}$.

5.2.2. Material properties

Our collisional modelling relies on assumptions about the material strength, determined by the material composition. If planetesimals were icier, they would be weaker than assumed here (Benz & Asphaug 1999; Wyatt & Dent 2002; Leinhardt & Stewart 2009). This would result in smaller critical projectile sizes and shorter collisional timescales. This, in turn, would result in larger planetesimal sizes and larger disc masses, possibly above the expected protoplanetary solid masses. Additionally, collisional damping of weaker bodies would be even less important.

Also determined by material composition is the dust opacity, which is used to infer the dust mass from the observed (sub)millimetre flux. We refer the reader to the discussion in Krivov & Wyatt (2021), who find that plausible variations in material composition would not drastically change inferred disc masses.

5.2.3. Size distribution

Our collisional masses depend strongly on assumptions about the size distribution. These enter the calculations through the extrapolation of dust mass to larger sizes, and also through the fragmentation timescale via the number of colliders.

The size distribution at millimetre sizes can be probed observationally through measurements of the spectral index at millimetre wavelengths. Typically, studies find a wide range of values, with samples ranging from 4 to 15 discs: $q = 3.36 - 3.50$ (Ricci et al. 2012, 2015), $q = 2.84 - 3.64$ (MacGregor et al. 2016), $q = 3.1 - 3.3$ (Marshall et al. 2017), $q = 3.2 - 3.7$ (Norfolk et al. 2021). From a sample of 133 discs, Marshall et al. (2026a) find the dust size distribution slope has a wide distribution with a peak around $q = 3.5$. For the discs in our sample they mostly find slopes very close to $q = 3.5$, with the exception of HD 197481, with $q = 3.1$. Therefore, the size distribution slope at dust sizes has a large scatter in observed discs. From the theoretical standpoint, we expect $q = 3.66$ for basalt and constant velocity dispersion (Benz & Asphaug 1999), as assumed in this work, or a steeper slope if collisional damping is important and velocity dispersion varies with size (Pan & Schlichting 2012).

The initial size distribution of planetesimals is much less certain. Planetesimal formation simulations give some predictions (e.g. Johansen et al. 2015; Simon et al. 2016; Schäfer et al. 2017; Gerbig & Li 2023), yet these are incongruent with our results – the disc mass problem discussed above. Additionally, the above studies have mostly focused on planetesimal sizes from gravitational collapse following streaming instabilities. Planetesimals may continue to evolve inside protoplanetary discs through mergers and through pebble accretion, which can re-shape their size distribution (e.g. Schlichting & Sari 2011; Schlichting et al. 2013; Johansen et al. 2015).

The inferred planetesimal sizes and corresponding disc masses depend not only on the assumed primordial power-law slope, but also on the size of the smallest primordial planetesimals. This is because the initial projectile-to-target size ratio has a huge effect on the initial fragmentation timescale. With an extreme assumption of a monodisperse (very narrow) initial distribution we found planetesimal sizes of only 10 cm to 10 m. Coincidentally, these are exactly the sizes we do not expect to

form through coagulation in protoplanetary discs, because of the well-known 'metre barrier' (Armitage 2010), and which might not be produced in great numbers by streaming instabilities either (Klahr & Schreiber 2020; Gerbig & Li 2023). On the one hand, this can be interpreted as a sign that the initial size distribution is not too narrow. On the other hand, our model does not take into account how early fragmentation and cratering/erosion might quickly produce smaller bodies, changing the size distribution early on. Time-dependent numerical collisional models are needed to explore this further.

5.2.4. Velocity evolution

In our collisional modelling, we assumed that the average collision velocity of planetesimals is constant throughout the system lifetime. This is contrary to our assumption that discs are self-stirred during their lifetimes, implying that (Ida & Makino 1993)

$$v_{\rm rel}(t) = v_{\rm rel}(t_{\rm age}) \left(\frac{t}{t_{\rm age}} \right)^{1/4}. \tag{30}$$

The fragmentation rate of planetesimals would be much smaller at early times, meaning that the planetesimals at the top of the cascade should be smaller than what we found. However, the correction factor can be roughly estimated by re-writing our condition for largest planetesimals in the cascade ($s_{\rm pl}$), $R_{\rm frag}(v_{\rm rel}(t_{\rm age}))t_{\rm age} = 1$ as

$$\int_0^{t_{\rm age}} R_{\rm frag}(v_{\rm rel}(t)) {\rm d}t = 1, \tag{31}$$

effectively averaging the fragmentation rate over the velocity history. Inserting Eq. (30) into Eq. (31), we find that the 'corrected' planetesimal size $s_{\rm pl}$ is only 10–35% smaller than inferred assuming constant collision velocity (for $q_{\rm p} = 3-4$). The corrected masses in planetesimals vary by the same factor. We note that we did not account for mass evolution over time because the mass of these largest possible planetesimals in the cascade remains close to their initial mass.

Furthermore, our assumed stirring rate is correct if the velocity dispersion of the stirrers is equal to that of the bodies being stirred, or smaller. This is true if the velocity of the stirrers and of the smaller bodies grows at the same rate, or the stirrers are cooled by dynamical friction. However, if collisional damping acting on the dust is efficient, it may reduce the excitation of the dust below that of the stirrers (Pan & Schlichting 2012). Alternatively, there could be one or more stirrers with stochastically larger eccentricities and/or inclinations; in such a case, secular effects might also become important (Costa et al. 2024).

Lastly, we might question if our assumptions about stirring and damping are self-consistent. Specifically, we assumed that collisional damping is inefficient at high velocities. Considering Eq. (30), it could be argued that if damping was efficient at some prior point in time, the dust velocity growth should have halted at a lower value. This apparent inconsistency is easily resolved if one considers that planetesimals' velocities would still have been steadily increasing. Ultimately, the 'early' dust is replaced by more recently produced dust with higher velocities.

5.3. Alternative stirring and damping mechanisms

Our assumption of stirrers embedded in discs, formed early on and stirring the debris from an initially zero velocity dispersion, yields reasonable results for the sizes and numbers of the stirrers. This does not guarantee that this scenario is indeed occurring in debris discs.

For example, many of the ARKS discs have a non-Gaussian vertical density distribution (Zawadzki et al. 2026), which is inconsistent with standard scattering theory where eccentricity and inclinations are in equipartition in the dispersion-dominated regime (Ida & Makino 1992). A companion ARKS paper shows that such non-Gaussian profiles can arise when scattering occurs in the dispersion-dominated regime when eccentricity and inclinations are *not* in equipartition, and instead eccentricities of either the debris or of the stirrer(s) are initially higher than the inclinations due to some other process (Chiang et al. 2026).

Furthermore, the growth of the stirrers may have been prolonged or perhaps is even still ongoing (Kenyon & Bromley 2002, 2004, 2008, 2010). Chiang et al. (2026) estimate that mergers are likely occurring among the stirrers in at least some ARKS discs. In this scenario, the stirrers had less time to stir the discs than assumed in our work, and the time period available for the planetesimals to have collided is shorter. The stirrers ought to be larger and/or more numerous than inferred in our work, and the planetesimals ought to be smaller (Krivov & Wyatt 2021).

An alternative scenario is that discs are stirred by external perturbers through secular perturbations. In this scenario, one must distinguish between the question of perturbers stirring the velocity dispersion up to the critical value required for the collisional cascade to form, and the question of perturbers stirring the vertical aspect ratios to their observed values. The former only requires particle eccentricities to be stirred (e.g. Mustill & Wyatt 2009; Pearce et al. 2022; Sefilian 2024), the latter requires a planet on an orbit initially inclined relative to the disc (e.g. Brady et al. 2023; Poblete et al. 2023; Sefilian et al. 2025). Stirring could also be 'mixed', caused by both internal and external big bodies (Muñoz-Gutiérrez et al. 2023; Marshall et al. 2026b), in which case the constraints derived here for the big bodies are upper limits. Vertical thicknesses of debris discs might also not be a product of gravitational interactions with planetary system bodies at all, and instead could be inherited from the protoplanetary disc phase (Walmswell et al. 2013), or induced by stellar flybys early on (Ida et al. 2000; Kalas et al. 2000).

Another possibly important omission in our work is the effect of gas, which is present in four discs in our sample: HD 39060, HD 9672, HD 32297, and HD 131835. If this gas is CO-dominated, second-generation gas, its density is too low to affect millimetre-sized dust grains (Olofsson et al. 2022). If, on the other hand, these discs contain massive remnants of protoplanetary gas, that gas would affect the aspect ratios measured at (sub)millimetre wavelengths (Youdin & Lithwick 2007; Olofsson et al. 2022; Marino et al. 2022).

6. Conclusions

We performed simple, semi-analytic collisional and dynamical modelling of a sample of 11 discs from the ARKS survey, whose vertical thicknesses are well constrained. Our findings are as follows:

1. The dust observed at millimetre wavelengths can be explained as products of steady-state collisional cascades with planetesimals ranging from a few metres to ten kilometres in size, with total masses contained in planetesimals of less than 200 $M_\oplus$. Larger planetesimals are not excluded by this modelling, but their presence may increase the disc mass above the expected mass budget of a planetary system.

2. The discs' vertical thicknesses can be explained by gravitational stirring in the dispersion-dominated regime by embedded large bodies, with collisional damping counter-balancing the stirring in only two systems. Stirrers' individual masses are always larger than those of the planetesimals, but their total mass need not be.

These results are consistent with expected masses of planetary systems. However, this is not a proof that the assumed processes indeed occur in debris discs. We see four ways to distinguish between different scenarios in the future. First, the population statistics could be improved by increasing the number of discs with well resolved vertical structure. We note, for example, that the ARKS survey found evidence of aspect ratios increasing with system age (Zawadzki et al. 2026), while the preceding REASONS survey (Matrà et al. 2025) with lower resolution data did not find any. Second, multiwavelength observations can constrain both the size distribution slope and the vertical structure dependence on the dust grain size (Vizgan et al. 2022; Han et al. 2026b). Third, in wider discs, the aspect ratio might vary with radius (Matrà et al. 2019; Han et al. 2025, Luppe et al., in prep.) and this should be explored in a larger sample. Fourth, Zawadzki et al. (2026) found that the majority of ARKS discs appear more likely to have a Lorentzian vertical density distribution, and not the Gaussian as is commonly assumed (including in this work). Observationally, confirming this finding in more discs and with higher quality data is a key to understand the processes shaping vertical structure. As for theory, models should go beyond simple predictions of the average collision velocity and make predictions for the inclination distribution in debris discs (as in e.g. Jankovic et al. 2024; Sefilian et al. 2025; Chiang et al. 2026).

Acknowledgements. We thank the referee for their detailed, constructive, and very useful comments. MRJ acknowledges funding provided by the Institute of Physics Belgrade, through the grant by the Ministry of Science, Technological Development, and Innovations of the Republic of Serbia. TDP was supported for this work by a UKRI Stephen Hawking Fellowship and a Warwick Prize Fellowship, the latter made possible by a generous philanthropic donation. AAS is supported by the Heising-Simons Foundation through a 51 Pegasi b Fellowship. EC is supported by the Simons Investigator program and the Miller Institute for Basic Research in Science, University of California, Berkeley. CdB acknowledges support from the Spanish Ministerio de Ciencia, Innovación y Universidades (MICIU) and the European Regional Development Fund (ERDF) under reference PID2023-153342NB-I00/10.13039/501100011033, from the Beatriz Galindo Senior Fellowship BG22/00166 funded by the MICIU, and the support from the Universidad de La Laguna (ULL) and the Consejería de Economía, Conocimiento y Empleo of the Gobierno de Canarias. SM acknowledges funding by the Royal Society through a Royal Society University Research Fellowship (URF-R1-221669) and the European Union through the FEED ERC project (grant number 101162711). Support for BZ was provided by The Brinson Foundation. AMH acknowledges support from the National Science Foundation under Grant No. AST-2307920. JPM acknowledges research support by the National Science and Technology Council of Taiwan under grant NSTC 112-2112-M-001-032-MY3. SMM acknowledges funding by the European Union through the E-BEANS ERC project (grant number 100117693), and by the Irish research Council (IRC) under grant number IRCLA- 2022-3788. Views and opinions expressed are however those of the author(s) only and do not necessarily reflect those of the European Union or the European Research Council Executive Agency. Neither the European Union nor the granting authority can be held responsible for them.

References

Armitage, P. J. 2010, Astrophysics of Planet Formation (Cambridge, UK: Cambridge University Press)
Backman, D. E. & Paresce, F. 1993, in Protostars and Planets III, ed. E. H. Levy & J. I. Lunine, 1253
Benz, W. & Asphaug, E. 1999, Icarus, 142, 5
Boccaletti, A., Thalmann, C., Lagrange, A.-M., et al. 2015, Nature, 526, 230
Boley, A. C., Payne, M. J., Corder, S., et al. 2012, ApJ, 750, L21
Brady, M. T., Faramaz-Gorka, V., Bryden, G., & Ertel, S. 2023, ApJ, 954, 14
Brahic, A. 1977, A&A, 54, 895
Brown, M. E. 2001, AJ, 121, 2804
Chiang, E. & Fung, J. 2017, ApJ, 848, 4
Chiang, E., Pearce, T. D., Jankovic, M. R., et al. 2026, ApJ, 1008, 163
Costa, T., Pearce, T. D., & Krivov, A. V. 2024, MNRAS, 527, 7317
Daley, C., Hughes, A. M., Carter, E. S., et al. 2019, ApJ, 875, 87
Farhat, M. A., Sefilian, A. A., & Touma, J. R. 2023, MNRAS, 521, 2067
Gerbig, K. & Li, R. 2023, ApJ, 949, 81
Goldreich, P., Lithwick, Y., & Sari, R. 2004, ApJ, 614, 497
Guzman, J., Murphy, J. W., Beasor, E., et al. 2026, ApJ, 1008, 99
Han, Y., Mansell, E., Jennings, J., et al. 2026a, A&A, 705, A196
Han, Y., Wyatt, M. C., Jankovic, M. R., et al. 2026b, A&A, 711, A42
Han, Y., Wyatt, M. C., & Marino, S. 2025, MNRAS, 537, 3839
Hornung, P., Pellat, R., & Barge, P. 1985, Icarus, 64, 295
Hughes, A. M., Duchêne, G., & Matthews, B. C. 2018, ARA&A, 56, 541
Ida, S., Larwood, J., & Burkert, A. 2000, ApJ, 528, 351
Ida, S. & Makino, J. 1992, Icarus, 96, 107
Ida, S. & Makino, J. 1993, Icarus, 106, 210
Jankovic, M. R., Wyatt, M. C., & Löhne, T. 2024, A&A, 691, A302
Johansen, A., Mac Low, M.-M., Lacerda, P., & Bizzarro, M. 2015, Science Advances, 1, 1500109
Kalas, P. 2005, ApJ, 635, L169
Kalas, P., Larwood, J., Smith, B. A., & Schultz, A. 2000, ApJ, 530, L133
Kenyon, S. J. & Bromley, B. C. 2002, ApJ, 577, L35
Kenyon, S. J. & Bromley, B. C. 2004, AJ, 127, 513
Kenyon, S. J. & Bromley, B. C. 2008, ApJS, 179, 451
Kenyon, S. J. & Bromley, B. C. 2010, ApJS, 188, 242
Klahr, H. & Schreiber, A. 2020, ApJ, 901, 54
Krivov, A. V. 2010, Research in Astronomy and Astrophysics, 10, 383
Krivov, A. V. & Booth, M. 2018, MNRAS, 479, 3300
Krivov, A. V., Ide, A., Löhne, T., Johansen, A., & Blum, J. 2018, MNRAS, 474, 2564
Krivov, A. V., Löhne, T., & Sremčević, M. 2006, A&A, 455, 509
Krivov, A. V. & Wyatt, M. C. 2021, MNRAS, 500, 718
Leinhardt, Z. M. & Stewart, S. T. 2009, Icarus, 199, 542
Lissauer, J. J. & Stewart, G. R. 1993, in Protostars and Planets III, ed. E. H. Levy & J. I. Lunine, 1061
Lodato, G., Dipierro, G., Ragusa, E., et al. 2019, MNRAS, 486, 453
Löhne, T., Krivov, A. V., Kirchschlager, F., Sende, J. A., & Wolf, S. 2017, A&A, 605, A7
Löhne, T., Krivov, A. V., & Rodmann, J. 2008, ApJ, 673, 1123
Lovell, J. B., Hales, A. S., Kennedy, G. M., et al. 2026, A&A, 705, A200
MacGregor, M. A., Wilner, D. J., Chandler, C., et al. 2016, ApJ, 823, 79
Marino, S. 2021, MNRAS, 503, 5100
Marino, S. 2023, in Planetary Systems Now, ed. L. M. Lara & D. Jewitt, 381–408
Marino, S., Cataldi, G., Jankovic, M. R., Matrà, L., & Wyatt, M. C. 2022, MNRAS, 515, 507
Marino, S., Matrà, L., Hughes, A. M., et al. 2026a, A&A, 705, A195
Marshall, J. P., Hengst, S., Young, R., et al. 2026a, MNRAS, 545, staf2221
Marshall, J. P., Maddison, S. T., Thilliez, E., et al. 2017, MNRAS, 468, 2719
Marshall, J. P., Muñoz-Gutiérrez, M. A., Sefilian, A. A., & Peimbert, A. 2026b, MNRAS, 545, staf1990
Matrà, L., MacGregor, M. A., Kalas, P., et al. 2017, ApJ, 842, 9
Matrà, L., Marino, S., Wilner, D. J., et al. 2025, A&A, 693, A151
Matrà, L., Wyatt, M. C., Wilner, D. J., et al. 2019, AJ, 157, 135
Matthews, B. C., Krivov, A. V., Wyatt, M. C., Bryden, G., & Eiroa, C. 2014, in Protostars and Planets VI, ed. H. Beuther, R. S. Klessen, C. P. Dullemond, & T. Henning, 521–544
Muñoz-Gutiérrez, M. A., Marshall, J. P., & Peimbert, A. 2023, MNRAS, 520, 3218
Mustill, A. J. & Wyatt, M. C. 2009, MNRAS, 399, 1403
Nesvold, E. R., Naoz, S., & Fitzgerald, M. P. 2017, ApJ, 837, L6
Norfolk, B. J., Maddison, S. T., Marshall, J. P., et al. 2021, MNRAS, 507, 3139
O'Brien, D. P. & Greenberg, R. 2003, Icarus, 164, 334
Olofsson, J., Thébault, P., Kral, Q., et al. 2022, MNRAS, 513, 713
Pan, M. & Sari, R. 2005, Icarus, 173, 342
Pan, M. & Schlichting, H. E. 2012, ApJ, 747, 113
Pearce, T. D. 2026, in Encyclopedia of Astrophysics, Volume 1, Vol. 1, 270–287
Pearce, T. D., Krivov, A. V., Sefilian, A. A., et al. 2024, MNRAS, 527, 3876
Pearce, T. D., Launhardt, R., Ostermann, R., et al. 2022, A&A, 659, A135
Pearce, T. D., Löhne, T., & Krivov, A. V. 2025, MNRAS, 544, 1447
Poblete, P. P., Löhne, T., Pearce, T. D., & Sefilian, A. A. 2023, MNRAS, 526, 2017
Quillen, A. C., Morbidelli, A., & Moore, A. 2007, MNRAS, 380, 1642
Ricci, L., Maddison, S. T., Wilner, D., et al. 2015, ApJ, 813, 138
Ricci, L., Testi, L., Maddison, S. T., & Wilner, D. J. 2012, A&A, 539, L6
Rodigas, T. J., Debes, J. H., Hinz, P. M., et al. 2014, ApJ, 783, 21
Safronov, V. S. 1972, Evolution of the protoplanetary cloud and formation of the earth and planets. (Keter Publishing House)
Schäfer, U., Yang, C.-C., & Johansen, A. 2017, A&A, 597, A69

Schlichting, H. E. 2014, ApJ, 795, L15
Schlichting, H. E., Fuentes, C. I., & Trilling, D. E. 2013, AJ, 146, 36
Schlichting, H. E. & Sari, R. 2011, ApJ, 728, 68
Sefilian, A. A. 2024, ApJ, 966, 140
Sefilian, A. A., Kratter, K. M., Wyatt, M. C., et al. 2025, MNRAS, 543, 3123
Simon, J. B., Armitage, P. J., Li, R., & Youdin, A. N. 2016, ApJ, 822, 55
Stewart, G. R. & Ida, S. 2000, Icarus, 143, 28
Stewart, S. T. & Leinhardt, Z. M. 2009, ApJ, 691, L133
Strubbe, L. E. & Chiang, E. I. 2006, ApJ, 648, 652
Stuber, T. A., Löhne, T., & Wolf, S. 2023, A&A, 669, A3
Terrill, J., Marino, S., Booth, R. A., et al. 2023, MNRAS, 524, 1229
Thébault, P., Augereau, J. C., & Beust, H. 2003, A&A, 408, 775
Vizgan, D., Hughes, A. M., Carter, E. S., et al. 2022, ApJ, 935, 131
Walmswell, J., Clarke, C., & Cossins, P. 2013, MNRAS, 431, 1903
Williams, J. P. & Cieza, L. A. 2011, ARA&A, 49, 67
Wyatt, M. 2020, in The Trans-Neptunian Solar System, ed. D. Prialnik, M. A. Barucci, & L. Young (Elsevier), 351–376
Wyatt, M. C. 2008, ARA&A, 46, 339
Wyatt, M. C., Clarke, C. J., & Booth, M. 2011, Celestial Mechanics and Dynamical Astronomy, 111, 1
Wyatt, M. C. & Dent, W. R. F. 2002, MNRAS, 334, 589
Wyatt, M. C., Smith, R., Greaves, J. S., et al. 2007, ApJ, 658, 569
Youdin, A. N. & Lithwick, Y. 2007, Icarus, 192, 588
Zawadzki, B., Fehr, A., Hughes, A. M., et al. 2026, A&A, 705, A197

[1] Institute of Physics Belgrade, University of Belgrade, Pregrevica 118, 11080 Belgrade, Serbia
[2] Astrophysikalisches Institut und Universitätssternwarte, Friedrich-Schiller-Universität Jena, Schillergäßchen 2-3, 07745 Jena, Germany
[3] School of Physics, Trinity College Dublin, the University of Dublin, College Green, Dublin 2, Ireland
[4] Department of Physics, University of Warwick, Gibbet Hill Road, Coventry CV4 7AL, UK
[5] Department of Astronomy and Steward Observatory, The University of Arizona, 933 North Cherry Ave, Tucson, AZ, 85721, USA
[6] Institute of Astronomy, University of Cambridge, Madingley Road, Cambridge CB3 0HA, UK
[7] Department of Astronomy, University of California, Berkeley, Berkeley, CA 94720-3411, USA
[8] Instituto de Astrofísica de Canarias, Vía Láctea S/N, La Laguna, E-38200, Tenerife, Spain
[9] Departamento de Astrofísica, Universidad de La Laguna, La Laguna, E-38200, Tenerife, Spain
[10] Division of Geological and Planetary Sciences, California Institute of Technology, 1200 E. California Blvd., Pasadena, CA 91125, USA
[11] Department of Astronomy, Faculty of Mathematics, University of Belgrade, Studentski trg 16, 11000 Belgrade, Serbia
[12] Department of Physics and Astronomy, University of Exeter, Stocker Road, Exeter EX4 4QL, UK
[13] Department of Astronomy, Van Vleck Observatory, Wesleyan University, 96 Foss Hill Dr., Middletown, CT, 06459, USA
[14] Academia Sinica Institute of Astronomy and Astrophysics, 11F of AS/NTU Astronomy-Mathematics Building, No.1, Sect. 4, Roosevelt Rd, Taipei 106319, Taiwan.
[15] Max-Planck-Insitut für Astronomie, Königstuhl 17, 69117 Heidelberg, Germany
[16] Department of Earth, Planetary, and Space Sciences, The University of California, Los Angeles, 595 Charles E. Young Drive East, Los Angeles, CA 90095, USA
[17] Institut für Astrophysik, Universität Wien, Türkenschanzstraße 17, 1180 Wien, Austria
[18] Konkoly Observatory, HUN-REN Research Centre for Astronomy and Earth Sciences, MTA Centre of Excellence, Konkoly-Thege Miklós út 15-17, 1121 Budapest, Hungary
[19] Center for Astrophysics | Harvard & Smithsonian, 60 Garden St, Cambridge, MA 02138, USA

Appendix A: Data and symbol tables

Table A.1. Input data to our models (Marino et al. 2026a; Zawadzki et al. 2026), followed by results on the sizes and the masses in planetesimals feeding the collisional cascades.

Name	M_* [$M_\odot$]	L_* [$L_\odot$]	$t_{\rm age}$ [Myr]	f [$\times 10^{-4}$]	r [au]	Δr [au]	h	$M_{\rm dust}$ [$M_\oplus$]	$v_{\rm rel}$ [km s^{-1}]	$s_{\rm pl}(q_{\rm p}=3)$ [km]	$M_{\rm pl}(q_{\rm p}=3)$ [$M_\oplus$]
HD 10647	1.1	1.6	1700	2.6	104	65	0.053	0.03	0.6	3.9	9.7
HD 131835	1.7	8.9	16	23	77	65	0.022	0.45	0.3	0.6	23.3
HD 14055	2.2	29.0	300	0.89	169	162	0.054	0.05	0.6	0.02	0.2
HD 15115	1.4	3.7	45	4.7	81	14	0.022	0.07	0.3	1.0	5.6
HD 161868	2.1	24.0	300	0.65	121	134	0.19	0.03	2.6	1.7	5.5
HD 197481 (AU Mic)	0.6	0.1	23	3.9	34	13	0.0028	0.012	0.04	0.003	0.03
HD 32297	1.6	7.0	30	61	116	37	0.009	0.87	0.1	0.3	17.1
HD 39060 (β Pic)	1.7	8.7	23	25	104	97	0.112	0.12	1.5	0.4	4.6
HD 61005	0.9	0.6	45	25	72	36	0.015	0.15	0.2	0.4	4.3
HD 76582	1.6	9.9	1200	2	204	176	0.192	0.12	1.8	3.3	39.4
HD 9672 (49 Ceti)	2.0	15.0	45	7.2	135	158	0.046	0.21	0.6	0.02	0.9

Table A.2. Key parameters.

Symbol	Parameter
M_*	Stellar mass
L_*	Stellar luminosity
$t_{\rm age}$	Stellar age
f	Disc fractional luminosity
r	Disc central radius
Δr	Disc radial width
h	Disc aspect ratio
$M_{\rm dust}$	Dust mass
$\sqrt{\langle e^2 \rangle}$	Root mean square of particle orbital eccentricities
$\sqrt{\langle i^2 \rangle}$, $i_{\rm rms}$	Root mean square of particle orbital inclinations
$v_{\rm rel}$	Collision velocity
s	Particle size (radius)
$Q_{\rm D}^*(s, v_{\rm rel})$	Specific critical disruption energy
$2Q_{\rm D}^*/v_{\rm rel}^2$	Critical projectile-to-target mass ratio
$n(s)$	Differential size distribution
$M(s)$	Mass in unit log-bin of size around s
$s_{\rm t}$	Target size
$s_{\rm p}$	Projectile size
$s_{\rm c}$	Critical projectile size
$s_{\rm blowout}$	Blowout size from radiation pressure
$s_{\rm pl}$	Size of planetesimals feeding cascades
$q_{\rm s}$	Size distribution slope in the strength regime
$q_{\rm g}$	Size distribution slope in the gravity regime
$q_{\rm c}$	Size distribution slope around $s_{\rm c}$
$q_{\rm p}$	Primordial size distribution slope
$t_{\rm frag}$	Fragmentation timescale
$t_{\rm damp}$	Collisional damping timescale
$\rho_{\rm s}$	Bulk density of particles in the cascade
$\rho_{\rm stir}$	Bulk density of stirrers
$M_{\rm stir}$	Mass of individual stirrer
$\Sigma_{\rm stir}$	Surface density of stirrers

Appendix B: Additional figures

Figure B.1 shows the ratio of the fragmentation timescale and the orbital period, as function of particle size. In all discs, for mm-sized dust and larger particles, catastrophic disruption collisions occur on average on the timescale of at least ~ 100× the orbital timescale.

Appendix C: Derivation of stirring constraints

To derive constraints on properties of stirrer(s), we followed Matrà et al. (2019). We start from Eq. (4.1) from Ida & Makino (1993), which describes time evolution of the mean-square of particle eccentricities due to gravitational self-stirring, stirring from a protoplanet embedded in the disc and dynamical friction heating due to interaction with the protoplanet. As noted by Ida & Makino (1993), an analogous equation describes evolution of particle inclinations. Dynamical friction heating is at most as strong as viscous stirring (Goldreich et al. 2004), and we neglect it. We wish to consider the case of self-stirring, as well as the stirring by a protoplanet, as well as the case of stirring by a larger number of protoplanets or simply large bodies that are not planetesimals themselves. As shown by Ida & Makino (1993), these different scenarios can be considered in a unified manner. Neglecting a factor two difference between the rates in different scenarios, the stirring rate of the mean-square of inclinations is simply given by

$$\frac{\mathrm{d}\langle i^2\rangle}{\mathrm{d}t} = \frac{\langle i^2\rangle}{T_{\rm VS}}, \tag{C.1}$$

where $T_{\rm VS}$ is the viscous stirring timescale. From Ida & Makino (1993), in the dispersion-dominated regime the viscous timescale for the stirring of inclinations is given by their Eq. (4.2), replacing the numerical factor given therein for eccentricities with a factor $C_i = 2$ for inclinations,

$$T_{\rm VS} = \frac{1}{C_i}\left(\frac{\Omega_{\rm K}^2 r^3}{GM_{\rm stir}}\right)^2 \frac{\langle i^2\rangle^2}{\Sigma_{\rm stir}/M_{\rm stir}\times r^2\Omega_{\rm K}}. \tag{C.2}$$

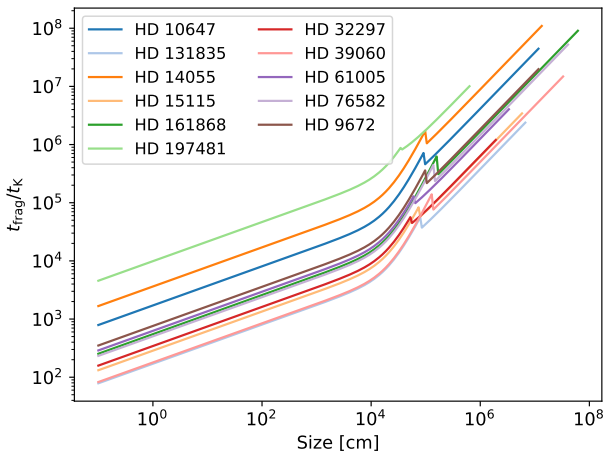


Fig. B.1. Ratio of the fragmentation timescale shown in the left panel of Fig. 2 and the orbital period ($t_{\rm K}$) as function of particle size for each of the discs. Lines are cut off at the upper end at the sizes at which the critical disruption energy becomes too large and the bodies cannot be catastrophically disrupted except in collisions with larger bodies.

This expression holds both in the case of self-stirring and in the case of a single large stirrer, only in the latter case the surface density is an effective surface density (see Eq. (4.8) in Ida & Makino 1993). In the stirring rate and in the constraint derived below we do not make this distinction, and instead take it into account as an additional constraint on the minimum surface density of stirrers, as in Eq. (21), following Matrà et al. (2019).

Inserting $T_{\rm VS}$ from Eq. (C.2) into Eq. (C.1), we obtain

$$\langle i^2\rangle \mathrm{d}\langle i^2\rangle = \frac{C_i G^2 M_{\rm stir}\Sigma_{\rm stir}}{\Omega_{\rm K}^3 r^4}\mathrm{d}t. \tag{C.3}$$

Integrating from $t = 0$ to $t = t_{\rm age}$ and from $\langle i^2\rangle(t = 0) = 0$ to the present-day value, assuming the spatial distribution and the sizes of the stirrers do not evolve, we obtain

$$\frac{\langle i^2\rangle^2}{2} = \frac{C_i G^2 M_{\rm stir}\Sigma_{\rm stir}}{\Omega_{\rm K}^3 r^4} t_{\rm age}. \tag{C.4}$$

Inserting $\langle i^2\rangle^2 = i_{\rm rms}^4$, C_i and $\Omega_{\rm K}$, and re-arranging, this equation yields the constraint on $M_{\rm stir}\Sigma_{\rm stir}$ in Eq. (20).

The constraint on the stirrer(s) in the shear-dominated regime is derived analogously. From Eq. (4.7) of Ida & Makino (1993), neglecting a factor of $2^{2/3}$ difference between the self-stirring and stirring by a single large stirrer, the viscous timescale is given by

$$T_{\rm VS,shear} = \frac{1}{C_i'}\left(\frac{\Omega_{\rm K}^2 r^3}{GM_{\rm stir}}\right)^{2/3} \frac{1}{\Sigma_{\rm stir}/M_{\rm stir}\times r^2\Omega_{\rm K}}, \tag{C.5}$$

where $C_i' = 3$. Inserting this into Eq. (C.1), assuming $i_{\rm rms}(t = 0) = i_0$, following the same steps as above and dropping the numerical pre-factor of an order of unity, we obtain Eq. (25).